Long-range correlation properties of quasi-coherent modes at TEXTOR

2015 New J. Phys. 17 073007

(http://iopscience.iop.org/1367-2630/17/7/073007)

New Journal of Physics
The open access journal at the forefront of physics

Deutsche Physikalische Gesellschaft DPG
IOP Institute of Physics

Published in partnership with: Deutsche Physikalische Gesellschaft and the Institute of Physics

OPEN ACCESS

RECEIVED
17 December 2014

REVISED
5 May 2015

ACCEPTED FOR PUBLICATION
18 May 2015

PUBLISHED
3 July 2015

PAPER

Long-range correlation properties of quasi-coherent modes at TEXTOR

A Krämer-Flecken[1], S Soldatov[2], Y Xu[3], H Arnichand[4], S Hacquin[4], R Sabot[4] and the TEXTOR team

[1] Institut für Energie- und Klimaforschung / Plasmaphysik, Forschungszentrum Jülich GmbH, D-52425 Jülich, Germany
[2] Karlsruhe Institute of Technology (KIT), Institut für Hochleistungsimpuls- und Mikrowellentechnik, 76344 Eggenstein-Leopoldshafen, Germany
[3] Southwestern Institute of Physics (SWIP) PO Box 432, Chengdu, Sichuan 610041, People's Republic of China
[4] CEA, IRFM, F-13108 Saint-Paul-Lez-Durance, France

E-mail: a.kraemer-flecken@fz-juelich.de

Keywords: microwave diagnostic, plasma turbulence, quasi-coherent modes, density fluctuations, plasma physics

Abstract

The paper reports on the first measurements of long-range correlations along field lines in the center of ohmic plasmas at TEXTOR. The measurements are performed with correlation reflectometry. For the first time the poloidal, toroidal and radial extension of quasi-coherent modes are simultaneously investigated using correlation reflectometry at two poloidally and toroidally separated positions. The experiments also allow the local determination of the toroidal velocity from a combination of delay time estimation and safety factor measurements from the same instrument. The paper investigates whether turbulence and which kind of turbulence, with respect to the frequency range, is aligned along field lines and embedded on iso-density surfaces in ohmic plasmas. It especially addresses the question of the properties of coherent structures in the vicinity of the $q = 1$ surface by analyzing propagation times and coherence levels from short- and long-range correlations. The results are discussed within the context of quasi-coherent modes as observed at T-10, TEXTOR, Tore Supra and recently JET and which are linked to trapped electron modes. Furthermore, the experiment tries to investigate whether a treatment of turbulence in two dimensions is sufficient or if 3D geometry has to be used for the description of turbulence stimulated transport. This is of importance for the development of turbulence codes and simulations.

1. Introduction

In general there exist two kind of long-range correlations: (i) those where the measurements are performed on a flux surface, independent of the poloidal angle and (ii) those which follow magnetic field lines. The following paper reports on the latter type. These experiments are difficult and need at least two toroidal separated observations points which are connected by a field line. For a diagnostic at two different poloidal and toroidal locations this condition is fulfilled for a certain combination of plasma current (I_p), toroidal magnetic field (B_t) and a certain radial position (R). Furthermore several quantities such as density and temperature can fluctuate along a magnetic field line. To make it more difficult the diagnostic must be fast enough to catch and follow structures within a decorrelation time of the turbulent structure which is in the order of several microseconds and small radial as well as poloidal wavelength of ≈0.01–0.04 m. Also some educated guess about the parallel correlation length is necessary to place the diagnostics not too far apart from each other.

Only a few publications report on experiments of long-range correlations (LRC). These experiments are mostly performed with two Langmuir probes at different poloidal and toroidal positions. Because of the short penetration depth of probes in the plasma the measurements are restricted to the plasma edge, only. First measurements of this kind date back to 1988 when Ritz and co-workers [1] investigated LRCs in the edge of TEXT tokamak. They reported a parallel wave number of $\langle k_\parallel \rangle = 0.015$ cm^{-1} at $q = 5.6$ with a probe set separated by $L_c = 1.18$ m. In 1999 Thomsen and co-workers [2] did experiments at JET using Langmuir probes as well.

The observed LRC for ion saturation current in the JET SOL for $q_{95} \approx 2.65$ and connection length of 22.6 m. A maximum correlation $\gamma_{\max} = 45\%$ and a delay time of $\Delta t \approx 20$ μs was observed. An upper limit for the parallel wave number was found to be 0.16 m^{-1} [3]. Similar experiments are performed at W7-AS [4]. The connection length between probe tips was $L_c = 6.3$ m and the delay time $\Delta t = 0.5$ μs which yields $k_{\|} \approx 0$ m^{-1}. An overview on further first experiments can also be found in the work of Endler [5]. In 2010 Grulke and co-workers reported on LRC measurements in the SOL of Alcator C-Mod [6] where they reported on a maximum correlation amplitude of 76% for a connection length of $L_c = 2.8$ m. At Russian tokamak T-10 LRC experiments with correlation reflectometry were performed for the first time [7]. Correlation reflectometry has the advantage of probing the plasma up to the core and therefore obtains information from regions deep in the plasma, where different mechanisms are responsible for the origin of the turbulence.

This paper will focus on the measurement and its interpretation of the long-range correlations of quasi-coherent structures along magnetic field lines in the vicinity of the $q = 1$ surface. It is organized as follows. The used diagnostic is shortly described in section 2. After a brief description of the experiment, measurement techniques and plasma conditions in section 3, the properties of the quasi-coherent structures will be presented in section 4. The structure of the quasi-coherent modes is discussed in section 5 and the main results are summarized in section 6.

2. Diagnostic set-up

The experiments are performed at TEXTOR, a medium-sized limiter tokamak ($R_0 = 1.75$ m, $a = 0.46$ m). TEXTOR is equipped with a heterodyne O-mode correlation reflectometer operating in the frequency range 26–40 GHz [8, 9]. The reflection layer is defined by the local electron density, guaranteeing that the reflection layer for the probing frequency is independent of the magnetic field. The system measures density fluctuations for $k_{\perp} \leqslant 3$ cm^{-1}. From the measured data turbulence properties and plasma rotation at three different locations (one top and two low field-side antennae arrays) are obtained. All antennae are pyramidal horns without focusing elements. The top array consists of four receiving antenna for measuring perpendicular plasma propagation ($v_{\perp}$), de-correlation time ($\tau_{\rm dc}$) and turbulence wavelength ($\lambda_{\perp}$) [10]. The two mid-plane arrays consist of four and two receiving horns, respectively. The array with two receiving antennae has the largest toroidal separation with respect to the top array and its antenna mouth has a square shape to allow O- and X-mode reflectometry. For the experiments reported here it is operated in O-mode together with the top array. The antennae of the low-field side (LFS) array are geometrical aligned in a way that the focal point of the array is located in the equatorial plane at R_0. The focal point for the antennae of the top array is located in the equatorial plane as well but shifted by 0.08 m towards the high field side. For both set-ups the observation of the $m = \pm 1$ diffraction order is not possible and resulting a Doppler shift of the whole spectrum is not observed. The experiments are performed with two reflectometers. Whereas the launcher of the top array can be fed by both, to measure in addition radial correlations the LFS launcher is served only by one reflectometer. For several discharges the second reflectometer is used in a frequency hopping operation to allow the measurement of radial correlations from the top array and a combination of long-range and radial correlations between both antennae arrays.

The reflected signal from top (four channels) and LFS array (two channels) are down-converted to 20 MHz and feed six IQ detectors. The output of the IQ detectors is digitized at a sample rate of 2 MHz. Data is taken during a time interval of 6 s starting with the discharge.

3. Plasma conditions

For the experiments reported here two antenna arrays are used, one on top of the vessel and another one in the outer equatorial plane (see figure 1). The angle in mathematical definition in toroidal direction between both arrays is $\Delta\Phi_{\rm geo} = 112.5°$. The top array is displaced by $s = 0.08$ m towards the high field side with respect to R_0. As a consequence the poloidal angle of this array increases with decreasing reflection layer radius (r_c) yielding $114 \leqslant \theta_{r_c} \leqslant 118°$ in the experiments under discussion. This causes a tilt angle for the launching top antennae of $24\,° \leqslant \theta_t \leqslant 28°$. The geometrical toroidal separation and the poloidal separation $\Delta\theta_{\rm geo}$ are in the same range matching the $q = 1$ condition.

To reach the $q = 1$ surface a low-density ($\bar{n}_e = 1.5 \times 10^{19}$ m^{-3}) and high-current ($I_p = 400$ kA) ohmic plasma at a magnetic field of $B_t = 1.9$ T is used to extent the operation range of the reflectometer towards the plasma center. For these conditions the plasma is in the linear ohmic confinement regime, where the confinement time increases linearly with the line averaged density. Therefore the existence of TEM-driven quasi-coherent modes is expected in the core plasma [11, 12]. Beside the absolute plasma parameters the

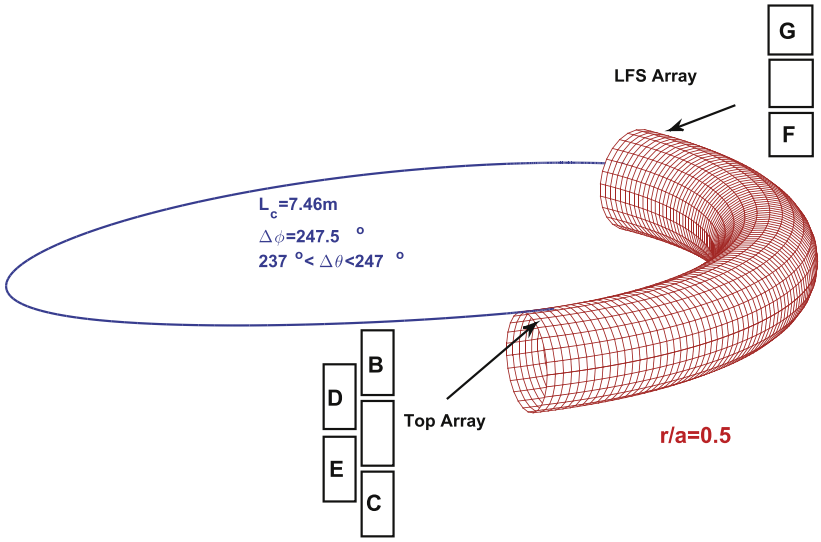

Figure 1. Sketch of the antenna arrays set. The arrangement and notation of the antenna in the array is shown, too. The solid line represents a magnetic field line and is a measure for the connection length between the arrays for $q = 1$ conditions at $r/a = 0.5$.

Table 1. Poloidal angles for the condition described above, when both reflectometers are probing the same iso-density layer.

Combination	CG	EG	DG	BG	CF	EF	DF	BF
Δ_{geo} [rad]	4.295	4.273	4.229	4.207	4.226	4.204	4.160	4.138

direction of I_p and B_t is important. In the case reported here I_p is in counterclockwise direction and B_t in clockwise direction when looking from above on the device. This connects the LFS array with the top array, also counterclockwise direction, with a connection length of $L_c = 7.46$ m and $\Delta\phi_{\mathrm{geo}} = 4.320$ rad as shown in figure 1. In this case the poloidal angle in radians of the different antennae combinations is calculated and shown in table 1 for the case that both reflectometers operate at the same frequency and reflection layer, respectively.

The data analysis is performed during the flat top of the discharge which lasts from 1–4 s. The time series of the complex amplitude for each antennae signal (Y_i) is constructed from the in-phase and quadrature component. Auto- and cross-correlation analysis is performed for time series (Y) from equal or different antennae within an array as well as in between the two arrays. The cross-correlation analysis yields the delay time (Δt),

$$\Delta t = \arg \max_t \Big(\big(|Y_i \star Y_j| \big)(t) \Big) \tag{1}$$

where the indices denotes a certain antennae. The maximum cross-correlation coefficient ($\gamma(\Delta t)$) is given as

$$\gamma(\Delta t) = \big(|Y_i \star Y_j| \big)(\Delta t) \tag{2}$$

and the correlation coefficient at zero delay (γ_0) as

$$\gamma_0 = \big(|Y_i \star Y_j| \big)(t = 0). \tag{3}$$

Displaying Δt as a function of the poloidal separation within either top or LFS array allows us to estimate the perpendicular rotation ($\Omega_\perp$) from the slope of the linear regression analysis for all antennae combinations as well as the perpendicular linear velocity $v_\perp = \Omega_\perp \cdot r_c$.

For the analysis the reflection layer is of importance, too. Here the HCN laser diagnostic at TEXTOR is used. It consists of nine channels which are used with an Abel inversion and the assumption of circular iso-density surfaces to calculate density profiles on a 10 ms standard time base. The assumption of circular iso-density surfaces excludes any poloidal asymmetry in the profile. The density profiles are assumed to be similar at both array positions. At the radial position of the measurement, the Shafranov shift amounts to 29 $\pm$ 3 mm.

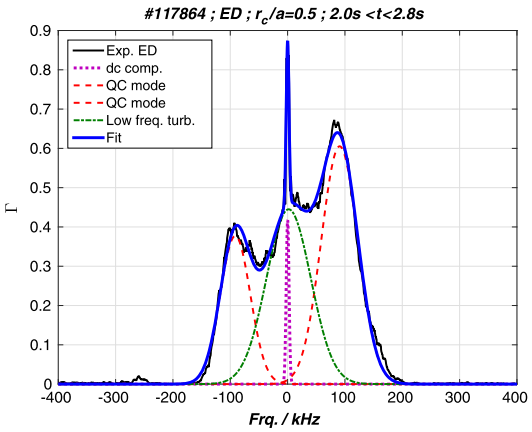

Figure 2. Averaged coherence for combination **ED** and its decomposition in different components. The measured spectrum and the approximated sum of the components are in good agreement

4. Results

This section describes the results obtained from short-range correlation (SRC) and long-range correlation (LRC) at $q \approx 1.0$ regarding the perpendicular rotation. In addition the turbulence properties, e.g. correlation length and de-correlation time, are investigated. The data reported here is collected during a period of 2 years and yields similar results which demonstrates the high reproducibility of the measurement and the reliability of the diagnostic as well as the robustness and reproducibility of the underlying physics.

The obtained results are ordered in sections. In section 4.1 short-range correlations at the top array are presented as far as they are necessary for the understanding of the LRC results. Section 4.2 ($\Delta r = 0$) shows the results for the LRC case with both reflectometer at the same flux surface and section 4.3 lists those results obtained for variable radial separation between the involved reflection layers.

4.1. General observations from short-range correlations

The turbulence complex amplitude spectrum in general is calculated from the Fourier transformation of small sample windows of 4 ms. To reduce the statistical noise, averaging for $20 \leqslant N \leqslant 100$ windows is performed. In case that the condition

$$\frac{\Delta\theta \cdot r_c}{v_\perp} < \tau_{\mathrm{dc}} \tag{4}$$

is fulfilled, where $v_\perp$ denotes the perpendicular velocity, r_c the reflection radius and τ_{dc} the de-correlation time of the turbulence, the magnitude squared coherence (Γ) spectrum defined as

$$\Gamma(f) = \frac{\left|G_{Y_iY_j}(f)\right|^2}{G_{Y_iY_i}(f) \cdot G_{Y_jY_j}(f)} \tag{5}$$

where $G_{Y_iY_i}(f)$ denotes the auto-spectral and cross-spectral density, respectively. The spectrum presents an overview of the turbulence at the location of the measurement. For the rest of the paper the word *coherence* is used to denote the magnitude squared coherence.

Following the discussion in [13] the complex amplitude spectrum is a super position of different components which can be described by Gaussian or Lorentzian shape. For the Γ-spectrum this decomposition can be done as well without the contribution of uncorrelated broad-band turbulence. For the plasma conditions outlined in section 3 the coherence spectrum can be decomposed into four Gaussians using the Levenberg–Marquardt algorithm by minimizing the weighted sum of squared residuals shown in figure 2 which shows the coherence spectrum for an antennae combination from the top array. Each single component can be described by a Gaussian shape. At zero frequency the dc component of the spectrum is seen which includes oscillations with rather low frequency, e.g. plasma position oscillations. Also centered at $f_c = 0$ kHz the low-frequency turbulence is found with a half width at half maximum (HWHM) of ≈40 kHz. Furthermore on both sides of the spectrum the quasi-coherent mode is found at $f_c \approx \pm 80$ kHz and a similar HWHM as for the low frequency turbulence. The centre frequency of the quasi-coherent mode as well as the amplitude of all components vary slightly when looking from the LFS array. With these three turbulence components the coherence spectrum is very well described.

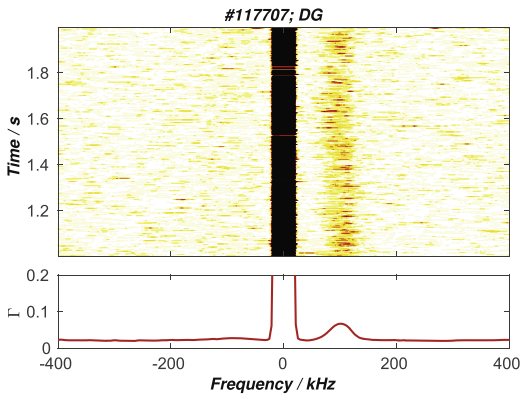

Figure 3. Coherence for LRC during flat top conditions showing the enhanced coherence in the range 80–120 kHz.

Table 2. Comparison of $\Omega_\perp$ for top, LFS and LRC conditions for different discharges. In addition an estimate of the local q from the top array is given.

#	$\Omega_\perp^{\mathrm{Top}}$ [krad s^{-1}]	$\Omega_\perp^{\mathrm{LFS}}$ [krad s^{-1}]	$\Omega_\perp^{\mathrm{LRC}}$ [krad s^{-1}]	r_c [m]	q_{Top}
113805	14.3	13.3	13.7	0.226	1.0 ± 0.1
117773	12.5	12.3	13.2	0.225	0.9 ± 0.15
117774	12.6	11.9	12.5	0.225	0.9 ± 0.2
117707	11.7	—	13.6	0.24	—
117864	12.1	12.1	11.9	0.227	1.0 ± 0.1

In the coherence spectrum an obvious asymmetry is observed. This asymmetry is caused by a rotation of fluctuations on the reflecting surface. The measured phase change $\mathrm{d}\Phi/\mathrm{d}t$ in a case without rotation is equal for the positive and negative frequency branches. An additional rotation changes $\mathrm{d}\Phi/\mathrm{d}t$ for the positive and negative branch and the asymmetry is observed. By changing the direction of the rotation, either by changing the direction of I_p or B_t, the asymmetry should change as well. Indeed this behavior is observed in the experiments.

4.2. Observations of LRC with $\Delta r = 0$

In the upper part of figure 3 the contour plot of the coherence (Γ) of the LRC combination **DG** is shown as function of frequency and time. A sample volume of 512 samples is used, 256 μs, respectively. Furthermore Γ is averaged for 5 windows. The spectrum is quite different to the one obtained for the SRC (see figure 2). It shows beside the dc component a high coherence level for 80 kHz $\leqslant f \leqslant$ 120 kHz above a low background level of $\gamma \approx 0.02$ for the rest of the frequency domain.

The coherence shows an intermittent and statistical behavior. The measured Γ varies in the range 0.02–0.28 , indicating that the density and the magnetic field are fluctuating quantities. The lower part of figure 3 shows the averaged coherence within the time window 1–2 s. A signal-to-background ratio of ≈3.5 is observed. The fact of a significant correlation for the positive branch only indicates a propagation of the underlying structure in counter-clock-wise direction and a parallel correlation length which is less than one toroidal turn or that the observed structure is not embedded in the iso-density surface probed by the two reflectometers. Besides the structure in the range 80 kHz $\leqslant f \leqslant$ 120 kHz no further structures are visible. That the low-frequency turbulence described by a Gaussian shape in figure 2 is entirely missing especially demonstrates that low-frequency turbulence has a different and much smaller correlation length.

To verify that the observed long-range correlation for $r/a = 0.52 \pm 0.01$ corresponds to the $q = 1$ surface, all delay times (Δt ($\Delta\theta$)) for the short-range correlation (SRC) within the top array are calculated. The delay time analysis is explained for discharge #117864 (see table 2). From the ratio of the obtained Δt values $q = 1.0 \pm 0.1$ is obtained using the method described in [8] and applied for all possible antennae combinations. In a next step Δt is calculated each 512 μs in the frequency range 50–152 kHz and for all 8 LRC combinations within the flat top of $1 \leqslant t \leqslant 3$ s.

In the upper part of figure 4 the probability distribution for $N = 7812$ Δt values as function of the time lag is shown for the combination **GD**. The single bin width is set to 1 μs. The data are approached by a Gaussian with a center at $\Delta t = 12.3$ μs which is assumed to be the mean propagation time. The same analysis for the SRC of the top array is shown in the lower part of figure 4. For this case Δt is much better determined. Note that in case of the LRC the poloidal distance is nearly a factor 4 larger than for the SRC case. Reasons for the broad distribution

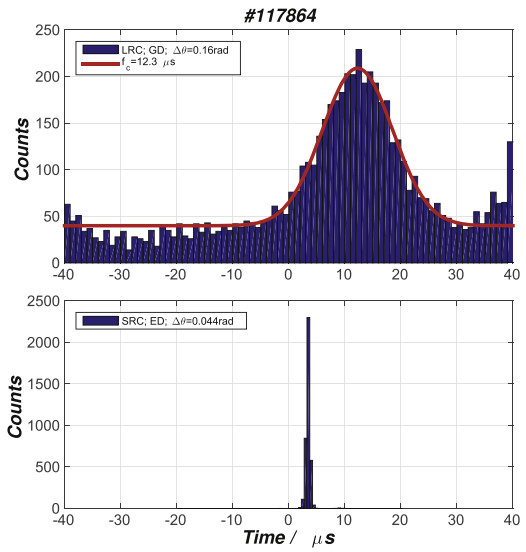

Figure 4. Upper part: PDF from the delay time estimation of the LRC combination *DG*. The solid line shows the Gaussian approximation of the PDF centered at $\Delta t = 12.3\ \mu$s. **Lower part:** same analysis for SRC combination **ED**.

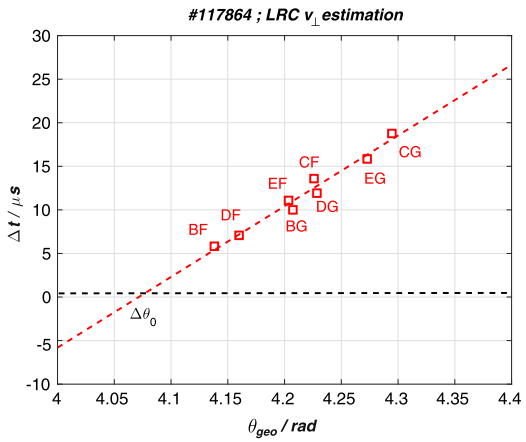

Figure 5. Δt as function of $\Delta\theta_{\mathrm{geo}}$. The estimated $\Delta\theta_0$ is shown as intersection with the $\Delta t = 0$ axis.

of Δt in the LRC case will be discussed later. Since the measurements are performed at the $q \approx 1$ surface effects of sawtooth could have an influence on the turbulence and the measured Δt. Therefore the sawtooth crash times are detected and the turbulence is investigated 1 ms before and after the sawtooth crash, where the largest difference in the profiles is expected. These time stamps are used in the calculation of Δt. Even for the bad statistics of only 500 analyzed events no significant difference in Δt before and after the sawtooth crash is found and any impact of sawtooth on the further analysis can be neglected.

For LRC conditions the mean propagation time as function of the geometrical poloidal angle $\Delta\theta_{\mathrm{geo}}$ is shown in figure 5. The Δt values from the LRC range from 5.6–18.7 μs. A value of $\Omega_\perp = 12.1$ krad s^{-1} is calculated which corresponds to a velocity of $v_\perp = 2.77 \pm 0.08$ km s^{-1}. Presenting the LRC Δt data as function of the geometrical poloidal angle, the effective poloidal angle is achieved from the linear approach as $\Delta\theta_0 = b/m$, where m and b denote the slope of the linear approach and the intersection with the Δt axis, respectively. In the case under discussion $\Delta\theta_0 = 4.072$ rad is estimated. The mean local $q(r_c)$ is calculated from

$$q(r_c) = \frac{(2\pi - \Delta\phi)\cdot m}{b}, \tag{6}$$

yielding a calculated value of $q(r_c) = 0.94$. The difference between $\Delta\theta_0$ and the geometrical poloidal distance of the antenna ($\Delta\theta_{\mathrm{geo}}$) is the effective poloidal distance, covered by the structure due to rotation. In figure 6 SRC and LRC data are shown as function of the effective $\Delta\theta$. Both data sets yield the same slope and $\Omega_\perp$. The partial overlap between the SRC data set (last 2 data points) and the LRC data set (first 2 data points) in figure 6 is perfect. Any toroidal propagation of the structures is not accessible from the Δt values, only.

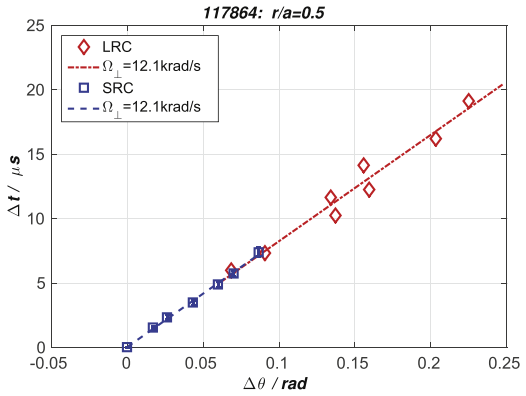

Figure 6. Estimation of $\Omega_\perp$ from SRC and LRC data set separately. Both data sets overlap partially and give the local q value. Note for the LRC data, $\Delta\theta = \Delta\theta_0 - \Delta\theta_{\mathrm{geo}}$.

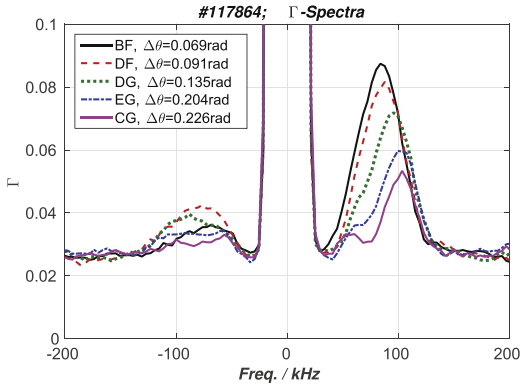

Figure 7. Coherence spectra obtained for different LRC combinations. $\Delta\theta$ denotes the real poloidal distance travelled by the structure.

The analysis is performed for several other discharges all yielding the same results. In table 2 $\Omega_\perp$ for top LFS and LRC conditions are summarized for several discharges. In all cases $\Omega_\perp$ is similar and shows that the result is independent of the used antenna array for SRC or LRC.

For the investigation of the coherence spectrum from the LRC combinations only those events are taken into account which lay within the full-width half-maximum of the Gaussian approaching the Δt distribution (see upper part of figure 4). With this conditional averaging all false events are neglected. According to equation (5) the Γ-spectrum for each combination is calculated from band pass–filtered raw data in the range 50–155 kHz for a sample volume of 512 samples and averaging over 4 windows. In figure 7 Γ-spectra for different combinations are shown. The strong asymmetry as in figure 3 is observed. Furthermore the center frequency f_{QC} as well as $\Gamma(f_{\mathrm{QC}})$ change with the LRC combination. The center frequency increases with increasing $\Delta\theta$ and Γ decreases with increasing $\Delta\theta$. Regarding the behavior of Γ it is similar to the observation for the SRC data.

The coherence spectra in figures 3 and 7 shows a remarkable asymmetry. Whereas the positive frequency branch shows a maximum in the range 70 kHz $\leqslant f_c \leqslant$ 100 kHz, no peak is found for the negative branch. This is in contrast to the observation for the short-range correlation where a broad peak in the coherence spectrum exist for the negative and positive frequency branch (see figure 8). The reason for the asymmetry is twofold. As discussed in section 4.1, an asymmetry in the coherence spectrum for the case of SRC is related to the rotation direction of the turbulence. Another reason could be the radial inclination or propagation of a structure with respect to the iso-density surface. Already in the work of Nazikian and Mazzucato [14] and Holzhauer and coworkers [15] it has been outlined that a radial propagation can lead to an asymmetry in the spectrum. However, it cannot be distinguished if the structure undergoes a radial propagation or inclination. In both cases an asymmetry should be observed. The observed asymmetry in figures 3 and 7 support a mismatch between an iso-density surface and the surface in which the structure is embedded.

In addition to $\Omega_\perp$, τ_{dc} characterizes the investigated structure. It is deduced from the top array only, because of the six different γ ($\Delta\theta$) which are approached by a Gaussian. In principle the de-correlation time for different types of turbulence can be different, therefore τ_{dc} is calculated for a filter (i) 50–150 kHz quasi-coherent mode

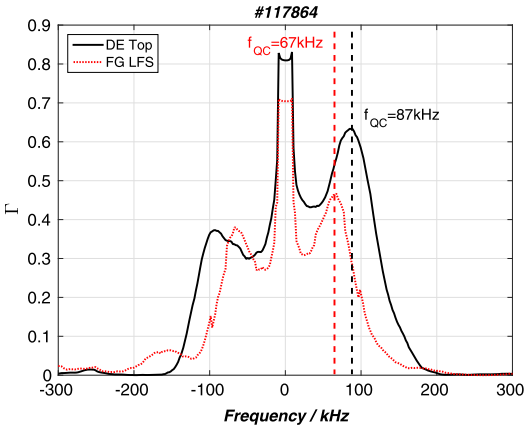

Figure 8. Coherence spectra for top and LFS showing the different peak position of the QC-mode.

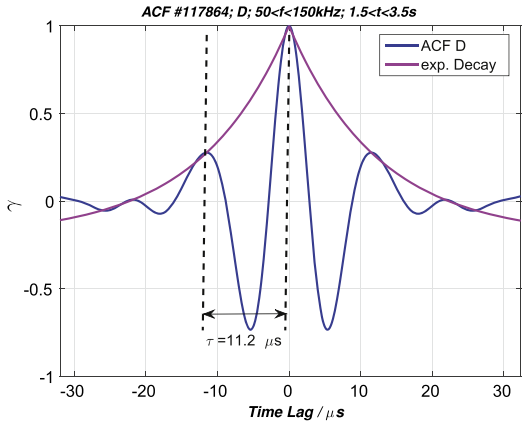

Figure 9. ACF for antennae D showing the oscillating structure of the turbulence in a poloidal plane.

only and (ii) 20–150 kHz low-frequency and quasi-coherent mode, yielding $\tau_{dc} = 14.8\ \mu s$ and $\tau_{dc} = 14.4\ \mu s$, respectively. Both values are obtained at the $1/e$-level of $\gamma_0(\theta)$ and which are in the same order or less than the measured Δt values from the LRC combinations. Furthermore it shows that the de-correlation time is similar for different types of turbulence and a factor of at least 15 smaller than the window size used for the Δt estimation.

The perpendicular structure length is obtained from the top array again. Therefore the auto-correlation function (ACF) from the top array is used. The full width at $1/e$-level of the ACF (w) is a measure for the perpendicular correlation length $L_\perp = w \cdot \Omega_\perp \cdot r_c$. The ACF for the previous defined conditions filtered for 50–150 kHz for top antennae **D** is shown in figure 9. The ACF shows an oscillating structure with a period of 11.2 μs. Two oscillations are observed on the positive and negative branches of the time lag, indicating a coherent structure. The period corresponds to a poloidal wave length of $\lambda_\perp = 32$ mm. The frequency of the structure corresponds nicely to the observed broad peak in the coherence spectrum. The exponentially decay of the oscillating structure yields an overall correlation length of $L_\perp = 63$ mm. Evidence for an oscillating structure is also found in the behavior of the Δt-traces for those antennae combinations with a mean $\Delta t > 5.3\ \mu s$. In this cases neighboring data volumes for Δt estimation exhibits jumps between two values separated by $\approx$5.6 μs without any change in the cross-correlation coefficient. Because the absolute value of the cross correlation coefficient is used to estimate Δt, the jumps occur already at the halfway period of the structure.

At the LFS and top the quasi-coherent mode dominates the Γ-spectrum (see figure 8). Here, the Γ-spectra for the combination **DE** ($\Delta\theta = 0.043$ rad) on top and **FG** ($\Delta\theta = 0.069$ rad) on LFS are shown. The mean spectra are obtained for 2.0 s $\leqslant t \leqslant$ 2.5 s. Both spectra show a broad structure above $f \geqslant 50$ kHz. The center frequency on the LFS is lower, yielding $f_{QC} \approx 65$ kHz compared to the top array where $f_{QC} \approx 87$ kHz is measured. It is interesting to note here that the QC-mode at the same iso-density surface has different f_{QC}. This points into the direction of a scaling with the local magnetic field squared which is a function of the major radius.

Table 3. Properties of QC modes at $r_c = 0.227$ m calculated from #117864.

Array	f_{QC} [kHz]	$v_\perp$ [km s^{-1}]	$\lambda_\perp^{QC}$ [mm]	$k_\perp$ [cm^{-1}]	$k_\perp \rho_i$
Top	87	2.8	32	2.0	0.54
LFS	65	2.8	42	1.5	0.36

The squared ratio of the major radius for the top and LFS array is 1.43 and the ratio of the f_{QC} yields 1.34 which is in fair agreement. Another estimate for the turbulence poloidal wave length comes from the relation $\lambda_\perp^{QC} = v_\perp / (f_{QC})$. For both poloidal positions the local properties are calculated and shown in table 3. For the calculation of $k_\perp \rho_i$ (ρ_i denotes the ion gyration radius), the central ion temperature is approximated by the Artsimovich [16] scaling with a shaping factor $f(r) = (1 - (r/a)^2)^2$. The $k_\perp \rho_i$ in both cases are in agreement with a TEM instability. This is consistent with the findings in [12] for TEXTOR and Tore Supra. Comparing both methods to determine $\lambda_\perp$ an overall agreement is found.

The coherent structures observed by Correlation Reflectometry are in general observable by Mirnov coils as well. However, Mirnov coils at TEXTOR are most sensitive to the plasma edge and therefore no simultaneous measurements of reflectometry and Mirnov coils could be performed in the vicinity of the $q = 1$ surface. At the edge Mirnov coils are sensitive to magnetic fluctuations. There, both diagnostics show the same broad peak due to the QC-modes. This suggests that QC-modes at $q = 1$ are accompanied by magnetic fluctuations which in a intuitive picture can be thought of current fluctuations.

4.3. Observations of LRC with $\Delta r \neq 0$

In this section one reflectometer is operating at slightly different frequencies to investigate radial extension of the turbulence and if the assumption of 2-dimensional symmetry in the plasma is fulfilled on the turbulence time scale. The latter is difficult, since the estimation of r_c is not on the turbulence time scale and therefore a mean r_c is used throughout the investigations. The reflectometer for the top array is either operated at larger r_c (smaller probing frequency) for the whole discharge or at several ascending radii during the flat top of the discharge investigating a radial range of $\Delta r = 60$ mm. These experiments are performed to investigate whether (i) the structure exhibits a radial outward propagation or (ii) the structure has an inclination in the $r - \phi$ plane. This analysis is complicated due to the varying distance between the center of the iso-density surface, when viewed in a poloidal plane and the intersection point of the top array sight-line with the equatorial plane (see section 3). It causes a coupling between $\Delta\theta$ and Δr. For increasing Δr, $\Delta\theta$ increases as well. This effect is taken into account in the following analysis.

The Δt values for a discharge with a radial separation of $\Delta r = 14$ mm is investigated. As in section 4.2, the PDF of all LRC combinations is calculated. In figure 10 the PDF is obtained from Δt-values calculated on 500 μs time window. The width of a single bin in the PDF is set to 1 μs. Instead of one peak up to four peaks become visible and are labeled from 1 to 4. Neighboring peaks are separated by $\approx$7 μs. Those peaks having the same label are approached by a linear function yielding all the same $\Omega_\perp$ (see figure 11). The offsets are different and poloidal shift between them is $\delta\theta = 0.083$ rad. The offset in $\Delta\theta$ translates to a poloidal distance at the reflection surface of $\approx$19 mm. This is just a similar distance when compared with half the poloidal wavelength as estimated from the autocorrelation analysis of antenna D shown in figure 9. The solid line in between the curves for labels 1 and 2 is the SRC for the same shot obtained for the top array. This fit fulfills the condition $\Delta t = 0$ μs for $\Delta\theta = 0$ rad. The observed difference in Δt ($\Delta\theta = 0$) with respect to the neighboring curves gives 4.2 μs and 2.2 μs, respectively. The ratio of both values is the ratio of the connection length from the LFS to the top array in the counterclockwise direction ($L_c = 7.5$ m) and in the clockwise direction ($L_c = 3.7$ m). The slope of the SRC data yields $\Omega_\perp = 11.0$ krad s^{-1} and is steeper than the slopes for the LRC with $\Omega_\perp = 13.4$ krad s^{-1}.

With a radial separation between the LFS and the outward directed top reflectometer of $\Delta r = 14$ mm, the measurement is just better aligned in the direction of the guiding line of the turbulence. Repeating the experiment for an inward $\Delta r = -10$ mm shows a complete loss of the correlation.

Conditional averaging for different peaks of one antennae combination and later Fourier transformation yields Γ-spectra where the center frequency does not vary, for the different peaks in the PDF. This is shown for the example in figure 12 for the combination **BG**. Within a time interval of $\pm$2.5 μs with respect to the peak maximum in the PDF (upper right panel in figure 10) all events are analyzed and averaged. The number of events for each peak varies between $N = 250$ for peaks 1 and 4 and $N = 630$ for peaks 2 and 3. The peak position in the Γ-spectrum is at $\approx$72 kHz for all four peaks of the PDF. The coherence level decreases with increasing Δt of the peak. The coherence per event is largest for the peak with $\Delta t = 4$ μs. For the negative frequency branch a significant coherence is also observed, which shows that with increasing Δr the two probing positions of the reflectometer more closely approach the alignment axis of the turbulent structure.

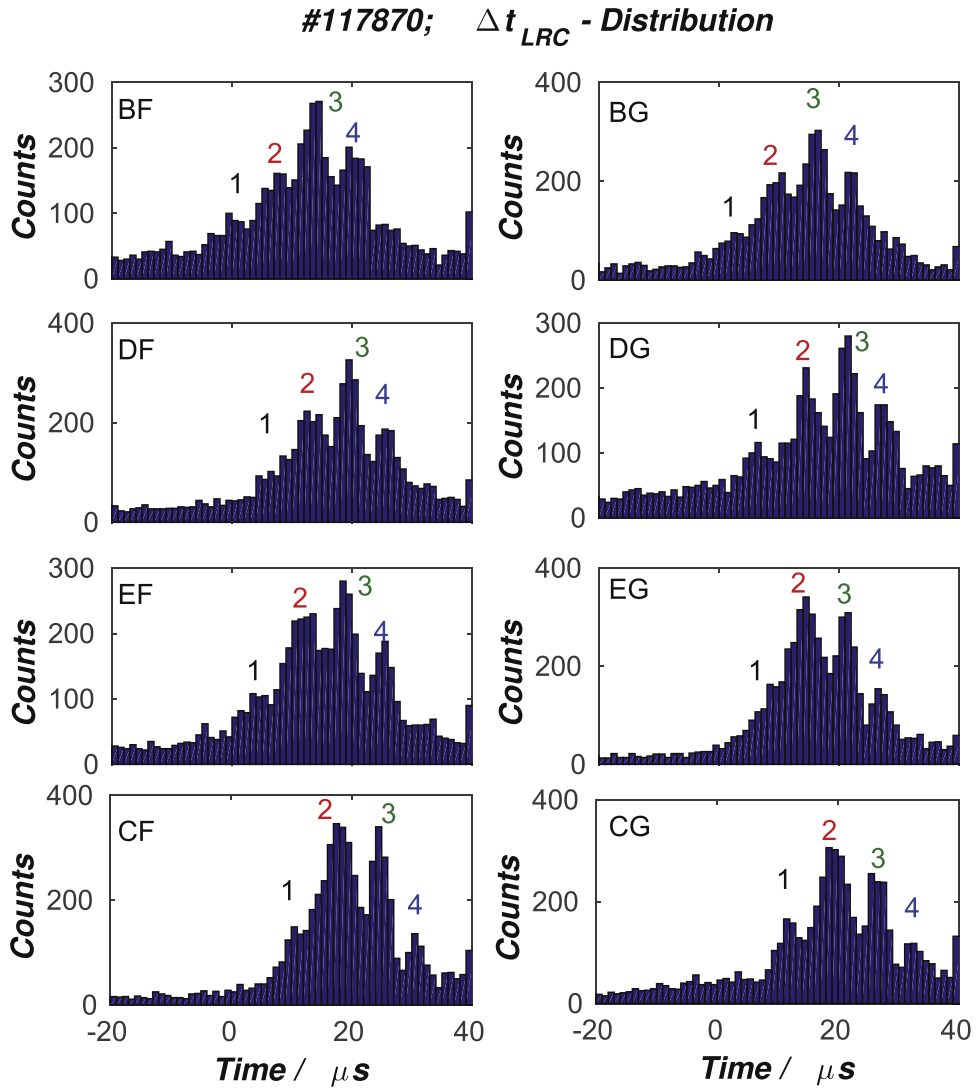

Figure 10. Distribution of Δt_{LRC} for #117870 with $\Delta r = 14$ mm. The Δt_{LRC} values are obtained each 500 μs. Clearly the different peaks are visible.

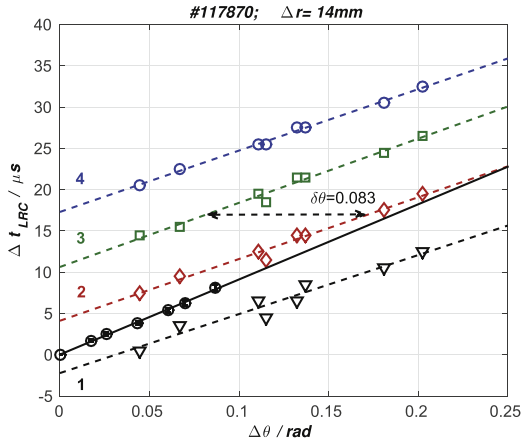

Figure 11. Δt-values for different peaks of figure 10. Labels are identical. Slopes (dashed lines) are equal for all four data sets. In addition the SRC data (black dots) are added.

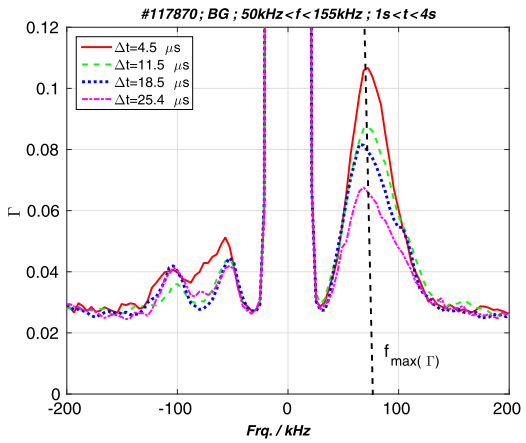

Figure 12. Coherence spectra for different Δt_{LRC}. The four dominate peaks are selected from combination **BG** shown in figure 10.

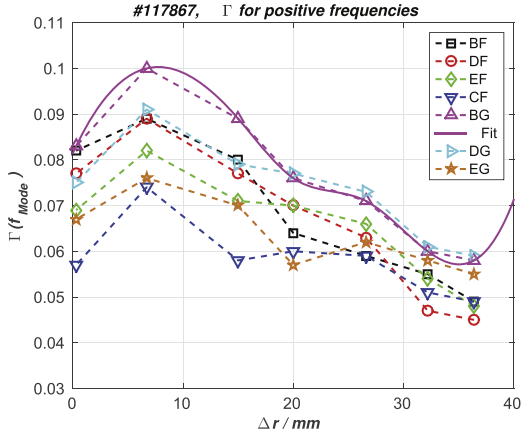

Figure 13. Coherence versus Δr shows that the turbulence has an outward directed inclination. No evidence for a radial propagation is found since the position of the maxmium does not change.

A scan of different radial positions within one discharge yields additional information on the asymmetry of the turbulence with respect to iso-density surfaces. The coherence spectra are calculated for radial range of $0 \leqslant \Delta r \leqslant 36$ mm and the coherence level at the mode frequency $\Gamma\,(f_{\mathrm{QC}})$ is deduced. The analysis distinguishes between the positive and negative frequency branches as discussed in section 4.2.

For the coherence in the positive frequency branch $\Gamma\,(f_{\mathrm{QC}})$ increases first with increasing Δr (see figure 13). For $\Delta r \geqslant 7$ mm, $\Gamma\,(f_{\mathrm{QC}})$ decreases. To estimate the maximum position the dataset for combination **BG** is approximated by a spline (solid line in figure 13). A flat maximum at $\Delta r = 8.2$ mm is estimated. This behavior is found for all antennae combinations and the result is taken as additional evidence that the turbulence is not embedded within a iso-density surface. A further point of interest is the fixed radial position for which the maximum in $\Gamma\,(f_{\mathrm{QC}})$ is achieved when looking at different combinations. Since each combination has a different poloidal propagation time, any additional radial propagation in the outward direction should result in a shift of $\Gamma\,(f_{\mathrm{QC}})$ towards larger radial separation. However, this is not the case and therefore either no radial propagation or a very small radial propagation is in agreement with this observation. An upper estimate is obtained for combinations **BF** and **EG**. For a radial propagation the peak for combination **EG** should observed at larger radial separation. A shift of half the radial separation ($\Delta r \approx 4$ mm) should already cause asymmetry in the shape of the peak in combination **EG**. The difference in the delay time δt is independent of the selected peak and yields for **BF** and **EG** is $\delta t = 10\ \mu$s. A radial velocity should be less than $v_r \ll \Delta r/\delta t = 400\ \mathrm{ms}^{-1}$ to be still comparable with the observations.

Analyzing the negative frequency branch shows a different behavior. As already mentioned earlier $\Gamma\,(f_{\mathrm{QC}})$ is comparable to the background Γ for $\Delta r = 0$ mm. However, at $\Delta r = 32$ mm a maximum in $\Gamma\,(f_{\mathrm{QC}})$ is found (see figure 14). For decreasing Δr, $\Gamma\,(f_{\mathrm{QC}})$ decreases as well. This result is fully in agreement with an inclination of the turbulence. Looking at the shape and maximum of $\Gamma\,(f_{\mathrm{QC}})$ for the negative frequency branch no

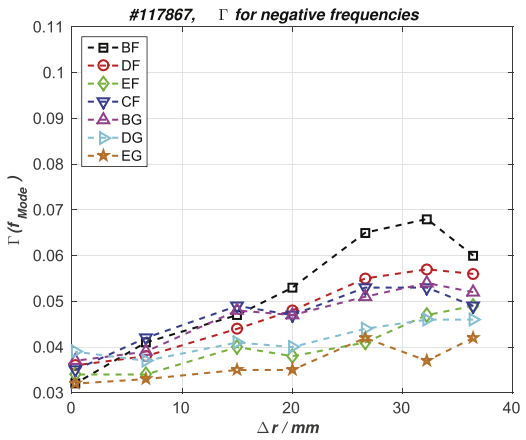

Figure 14. Coherence versus Δr for negative frequencies in agreement with outward directed inclination. Maximum in γ observed for $\Delta r = 32$ mm.

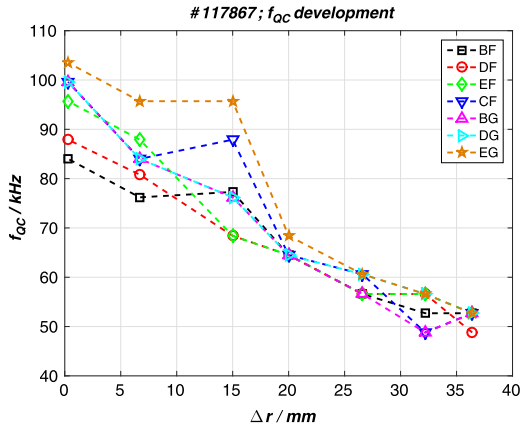

Figure 15. Development of the f_{QC}-mode frequencies with Δr.

indication of a movement of the maximum is found whereas a radial propagation can be neglected here as well. The usual asymmetry between positive and negative frequency branch observed for $\Delta r = 0$ mm disappears for a radial separation in the order of $\Delta r \approx 30$ mm. Both observations point towards a much larger effect due to the inclination of the turbulence than due to a possible small radial propagation.

Beside the radial distribution of $\Gamma\,(f_{\mathrm{QC}})$, the behavior of the mode frequency is of interest, too. For the positive frequency branch the mode frequency decreases with increasing Δr (see figure 15). For $\Delta r = 0$ mm a similar increase of the mode frequency with increasing $\Delta\theta$ is found as shown in figure 3. With increasing Δr this separation of the mode frequency decreases for the different combinations.

For the largest Δr the frequency drops well below the measured mode frequency obtained from SRC for either LFS or top array. In figure 16 $\Gamma\,(f_{\mathrm{QC}})$ is shown as a function of Δr and frequency. Here, the combination **BG** is chosen as an example. Because the variation in $\Delta\theta$ of the different LRC combinations is small with ($\Delta\theta_{\mathrm{max}} \leqslant 15\,°$) all other combinations show a similar behavior: (i) the asymmetric behavior for a high-frequency mode ($f \approx 100$ kHz) with a maximum at about $\Delta r = 8.2$ mm and (ii) the existence of a low-frequency mode ($f \approx 50$ kHz) which reaches its maximum at $\Delta r = 32$ mm. For the latter one the connection between the points of reflection is better aligned with respect to the alignment axis of the turbulence and a similar coherence level is observed on the negative and positive frequency branches. Furthermore the radial separation at the low frequencies is much larger compared to the high frequencies. However, both propagate with the same poloidal speed, intersecting the probed reflection layer under different angles.

From a couple of discharges the radial correlation is measured within the top antennae. Therefore antenna **C** is used for the hopping operation of one reflectometer. The other antennae are connected to the second reflectometer operating at constant frequency. A fast decrease of the coherence with increasing Δr is observed. Already at $\Delta r = 13.5$ mm the coherence for the QC-mode has become low (see figure 17(a)). Note that the reflection layer of the first reflectometer is varied with time. The figure has been achieved for a sample window of

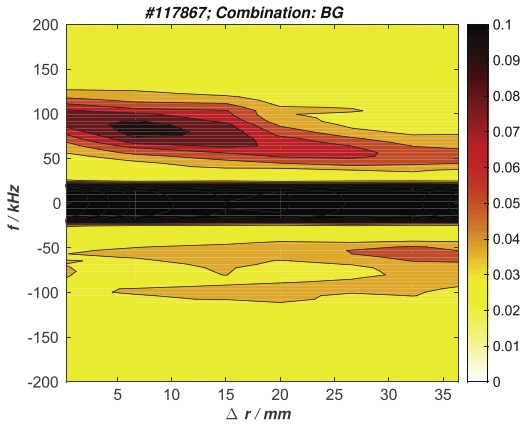

Figure 16. Contour plot of $\Gamma\,(f_{\mathrm{QC}})$ for combination **BG**, showing the different radial behavior of low- and high-frequency modes.

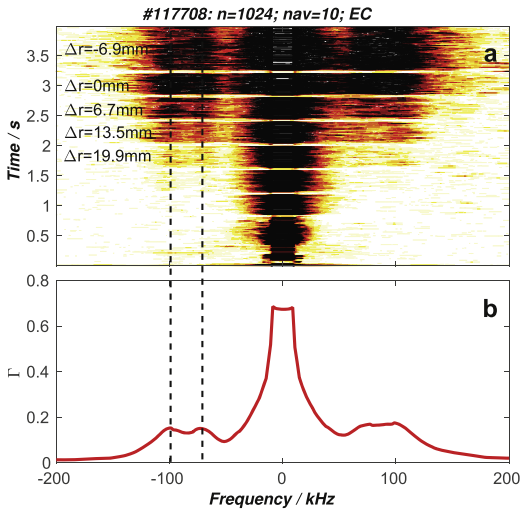

Figure 17. (**a**) Coherence for different radial separations within the top array. Note the fast radial decay. (**b**) Coherence level showing the two mode frequencies at ≈100 kHz and ≈70 kHz.

1024 and additional averaging of 10 windows. Moreover two frequencies can be identified in figure 17(b). The higher frequency perfectly matches with the one measured for the LRC ($\Delta r \approx 0$ mm). The lower one is significantly higher than the one measured for LRC ($\Delta r \approx 30$ mm). However, both frequencies are radially not separated in the SRC compared to the LRC. This should be interpreted that the inclination in the $r - \phi$ plane of the structures represented by the frequencies is different. However, a detailed radial scan for SRC and LRC is needed for better support of this statement. The observed radial decrease of the mode frequency goes along with an increase of the poloidal size of the mode. Evidence for a increase of the poloidal size of the mode is also found in the Δt distribution where the difference between neighboring peaks increases with Δr. As mentioned above an estimate of the structure size is given by $\lambda_\perp = v_\perp / f_{\mathrm{QC}}$. The perpendicular velocity in the investigated radial range is decreasing with increasing r_c, as discussed in [10], indicating that the plasma behaves not like a rigid body. Taking this into account $\lambda_\perp = 28$ mm is found at the innermost position and $\lambda_\perp = 48$ mm at the outermost position. The decrease in the mode frequency also explains the broad mode structure in the SRC measurements. In this case all possible modes contribute and form the broad structure in the frequency spectrum.

5. Discussion

One of the important questions which stood at the beginning of the investigation was whether it is possible to deduce the toroidal velocity from the LRC data. As shown in section 4.2, no information from the Δt-values on the parallel propagation can be obtained. However, as the local safety factor can be determined from the LRC

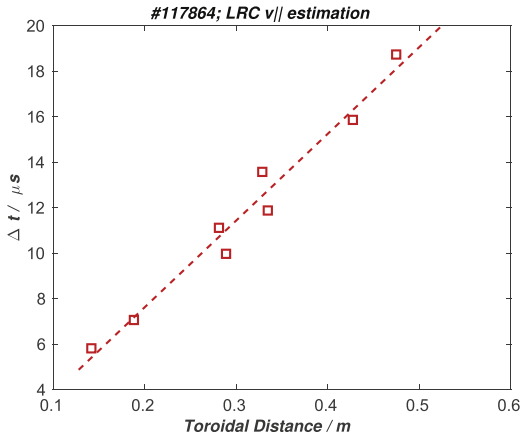

Figure 18. Estimate v_ϕ from the slope of the linear regression (dashed line in the figure).

data the effective poloidal and toroidal angles traveled by the turbulence can be deduced. Having determined the toroidal distance $s = \Delta\phi \cdot R_c$, where R_c is the major radius and $\Delta\phi = \Delta\theta/q$, the toroidal velocity (v_ϕ) can be calculated by linear regression of the data (see figure 18). In the discussed case $v_\phi = 26$ km s^{-1} is calculated. This value is in the same order as calculated from MHD analysis at the $q = 1$ of TEXTOR ohmic discharges [17]. In this thesis the comparison of v_ϕ derived within the framework of neoclassical theory and v_ϕ calculated from MHD modes are compared and a good agreement is achieved. With the $q = 1$ sawtooth precursor frequency and the central electron temperature v_ϕ is calculated for the discharge under discussion and compared with the toroidal propagation of the turbulent structure. A fair agreement is obtained. It demonstrates that the measurement of long-range correlation with correlation reflectometry can also give information on the toroidal velocity. The method can be applied in ohmic heated discharges and other cases where the standard v_ϕ measurements are not available.

Furthermore the question is discussed of the 3-dimensional structure of the mode with the help of the observations described in the previous sections. The important question is if the observed structure in the coherence spectrum at frequencies 50 kHz $\leqslant f \leqslant$ 100 kHz is really a coherent mode. From the definition of coherent modes given in [18], a fixed phase relation between vortices is a precondition. This seems to be the case when looking at the ACF of one antenna (see figure 9) which shows an oscillating structure. It is furthermore confirmed by the observed jumps in the time traces of Δt where jumps of ≈5.5 μs are observed. However, all these measurements are done in a poloidal cross section neglecting the toriodal dimension. The analysis of LRC at the same reflection layer does not add much more information beside a confirmation for the local q-value of the structure. However, LRC measurements performed for $\Delta r > 0$ mm add further relevant information on the structure size and toroidal extension. First of all the existence of several peaks in the Δt distribution, all equidistant for the same Δr, suggest the structure winds several times along the torus surface. In this sense the oscillating behavior in the ACF (see figure 9) is nothing other than the poloidal projection of a toroidally structure with at least two toroidal turns. The poloidal displacement for a full toroidal turn is given by $\delta\theta_q = (q_{\mathrm{LRC}} - 1) \cdot 2\pi = 0.38$ rad. However, the measured poloidal displacement from two consecutive toroidal turns is $2 \cdot \delta\theta = 0.17$ rad, which is only half the expected poloidal displacement and in contradiction with the hypothesis of several toroidal turns, suggests a deviation from a magnetic field line. Further evidence for a deviation from magnetic field lines comes from the observation that the structure exhibits an outward radial displacement. The maximum in the coherence is found for $\Delta r \approx 8$ mm which also indicates a mismatch between iso-density surfaces and flux surfaces.

The poloidal size of the structure is given by $\lambda_\perp = \tau \cdot v_\perp = 31$ mm for $\Delta r = 0$ mm. On the other hand the Δt distribution suggests (see figure 10) $\lambda_\perp = \delta t \cdot v_\perp = 38$ mm, where δt is twice the time between neighbouring peaks in the distribution. The observed discrepancy can be explained by the fact that τ is determined from SRC data, whereas δt comes from LRC data.

Another possibility of interpreting the multi-peak structure in the PDF for $\Delta r > 0$ mm is the fact that the different linear interpolations shown in figure 11 correspond to slightly different $q(r_c)$ of 0.86–0.95 , using the method as discussed for figure 5 by calculating $\Delta\theta_0$ for all four lines of figure 11. A variation in $q(r_c)$ can be caused by a fluctuating plasma current, which in turn causes a fluctuating poloidal magnetic field. This argument is to some extent confirmed by observations from Mirnov coils at the plasma edge, showing in the Fourier spectrum a broad structure at similar frequencies as observed by reflectometry. Unfortunately such

measurements are not available at the $q = 1$ surface and therefore cannot be compared directly with the spectra from correlation reflectometry.

Looking at the number of counts in the Δt distribution (see figure 10) for different peaks shows a large variation. This indicates a wide spread in $L_\parallel$ for individual structures. However, this effect is to a certain extent masked by a radial fluctuation of the reflection layer, which is demonstrated when gating on one peak and one antennae combination in the Δt distribution and looking for the resulting Δt distribution of the other combinations. In this case all other combinations should show the gated peak in the distribution, only. However, the distribution shows again all peaks which is interpreted as a sign for fluctuations of r_c or as mentioned above due to fluctuation in the plasma current.

The fact that the multi-peak structure in the PDF of Δt is not seen in the case of $\Delta r = 0$ mm comes from a combination of (i) an inclination of the guiding line of the structure with respect to the iso-density surface and (ii) the decreased period between single peaks due to an increase of the mode frequency. Therefore it is evidence for a discrepancy between iso-density surfaces and field line structure of the turbulence, assuming that iso-density surfaces and magnetic flux surface are similar.

An estimate of the toroidal correlation length under these conditions is difficult. It varies between one and two toroidal turns. Therefore $11\ \text{m} \leqslant L_\parallel = n \cdot 2\pi R_c \leqslant 22\ \text{m}$. The corresponding parallel wave number $k_\parallel$ varies between $0.003\ \text{cm}^{-1} \leqslant k_\parallel \leqslant 0.006\ \text{cm}^{-1}$.

From the performed experiment the observed structure can be treated as a coherent or quasi-coherent structure or mode as is discussed in [18]. However, more experiments with a higher time resolution and less radial separation are are needed to solve this question as well to give an adequate number for the toroidal correlation length.

6. Summary

The paper reports on experiments at TEXTOR which aim to investigate the long-range correlation (LRC) of so-called quasi-coherent (QC) modes. The main diagnostic tool in the experiment is a correlation reflectometer, measuring density fluctuations on two different poloidal and toroidal separated positions. The achieved results from correlation reflectometry show nicely the progress and general capability of this diagnostic for the detailed study of turbulence as well as the capability of micro-wave diagnostics for future fusion devices. In particular, the non-pertubative determination of the toroidal velocity opens new possibilities for those plasma conditions where other diagnostics for v_ϕ (e.g. charge exchange) are not available.

According to the positions of the diagnostic and plasma conditions, QC modes are studied at $\bar{q} = 1.0$. From the analysis of the squared coherence (Γ) a correlation for a connection length of 7.5 m is found for frequencies 50–150 kHz. The observed asymmetry in the spectrum is interpreted as a mismatch between the symmetry axis of the mode and the observation axis given by the reflection layer of the instrument. The observation of a significant coherence for frequencies 50–150 kHz shows that low-frequency turbulence, dominating the spectrum for short-range correlations, has much smaller or no parallel correlation length. Furthermore the LRC of QC-modes shows no continuous feature in time as e.g. poloidal correlations but does show, a statistical character. Averaging over large time intervals will extinguish the LRC due to an arbitrary phase relation between individual events.

The statistical analysis of the propagation time from all two-point combinations yields a broad distribution in the case of LRC, compared to the sharp peak in SRC. The evaluated propagation time from the probability distribution for each LRC combination as function of the poloidal separation yields a linear relation whose slope is in good agreement with the poloidal rotation estimated from the SRC combinations. However, the LRC combinations offer a further possibility to estimate local q in addition, which is in good agreement with the one estimated from the SRC combinations.

Operating both reflectometer with a frequency difference is used to study the alignment of the QC-modes with respect to iso-density surfaces. In those experiments the radial development of the maximum coherence at the frequency of the mode is investigated. No evidence for a significant radial propagation ($v_r \ll 400\ \text{m s}^{-1}$) of the mode is found, since the maximum of the coherence for different combinations, which corresponds to different propagation times does not change. However, an inclination of the QC modes in the $r - \phi$ plane is found.

In addition the Δt distribution shows several equidistant peaks. For each peak and all LRC combinations a local q can be determined. This suggests that the different peaks may come from fluctuations of the plasma current which causes fluctuations in the poloidal magnetic field. This would be in agreement with the observation by Mirnov coils which see QC-modes at similar frequency as the correlation reflectometer, but not at the same radial position. It is an indication that the QC-modes carry small amounts of plasma current and can

be interpreted as current filaments. This topic should be investigated in the future to study the correlation between density and magnetic fluctuations.

The perpendicular structure ($L_\perp$) of the quasi-coherent mode is estimated either from the auto correlation (AC) of different antenna showing an oscillating structure with a wavelength of 30 mm or from the distance between peaks in the Δt distribution for the cases with $\Delta r > 0$ mm. The method based on the perpendicular velocity divided by the QC-mode peak position in the coherence spectrum yields similar values for $\lambda_\perp$. All three measurements are in agreement. The measurements are performed in the linear confinement regime in the vicinity of the $q = 1$ surface where the mode frequency is in the range 50 kHz $\leqslant f_{QC} \leqslant$ 150 kHz and the normalized scale is $k_\perp \rho_i \approx 0.5$. A correlation between the mode and the TEM-dominated regime has been recently as shown for TEXTOR and Tore Supra [12]. The parallel correlation length ($L_\parallel$) is deduced to 11 m $\leqslant L_\parallel =$ 22 m which corresponds to 1–2 toroidal turns.

Furthermore the QC-modes seems to consist of at least two major frequencies, one at ≈100 kHz and the other at ≈60 kHz. Both modes have the same poloidal propagation speed but obviously different inclination due to different radial behavior. All these observations provide evidence for a 3-dimensional nature of turbulence. This may have also influence the transport in the plasma. At least QC-modes do not propagate on iso-density surfaces but are observed even when the radial displacement is about 35 mm, which is much more than the radial correlation length. Even taking into account that flux surfaces and iso-density surfaces may differ the observed radial displacement is too high to justify the statement that the turbulence is propagating on flux surfaces. This should be taken into account in future transport simulations.

Acknowledgments

This work was performed in the framework of the Helmholtz Virtual Institute on plasma dynamical processes and turbulence using advanced microwave diagnostics. The views and opinions expressed herein do not necessarily reflect those of the European Commission.

References

[1] Ritz C P *et al* 1988 *Rev. Sci. Instrum.* **59** 1739–44
[2] Thomsen H *et al* 1999 *26th EPS Conf. Control. Fusion and Plasma Phys.* **ECA 23J** 1541–4 (http://epsppd.epfl.ch/Maas/web/pdf/p4045.pdf)
[3] Thomsen H *et al* 2002 *Phys. Plasmas* **9** 1233–40
[4] Bleuel J, Endler M, Niedermeyer H, Thomsen H, Schubert M The W7-AS Team 2002 *New J. Phys.* **4** 38
[5] Endler M 1999 *J. Nucl. Mater.* **266–269** 84–90
[6] Grulke O, Terry J L, LaBombard B, Cziegler I and Zweben S J 2010 *37th EPS Conf. Control. Fusion and Plasma Phys.* **34A** P1.1036 (http://ocs.ciemat.es/EPS2010PAP/pdf/P1.1036.pdf)
[7] Vershkov V A, Soldatov S V, Shelukhin D A and Chistiakov V V 1999 *Nucl. Fusion* **39** 1775
[8] Krämer-Flecken A, Soldatov S, Vowinkel B and Müller P 2010 *Rev. Sci. Instrum.* **81** 113502
[9] Soldatov S, Krämer-Flecken A and Zorenko O 2011 *Rev. Sci. Instrum.* **82** 033513
[10] Krämer-Flecken A, Dreval V, Soldatov S, Rogister A, Vershkov V and the TEXTOR-team 2004 *Nucl. Fusion* **44** 1143–57
[11] Rice J E *et al* 2011 *Pvhs. Rev. Lett.* **107** 265001
[12] Arnichand H *et al* 2014 *Nucl. Fusion* **54** 123017
[13] Vershkov V A *et al* 2011 *Nucl. Fusion* **51** 094019
[14] Nazikian R and Mazzucato E 1995 *Rev. Sci. Instrum.* **1** 392–8
[15] Holzhauer E, Hirsch M, Grossmann T, Branas B and Serra F 1998 *Plasma Phys. Control. Fusion* **40** 1869–86
[16] Gott Yu V 2007 *Plasma Phy. Rep.* **33** 880
[17] de Bock M 2007 Understanding and controlling plasma rotation in tokamaks *PhD Thesis* Technische Universiteit Eindhoven Netherlands (http://alexandria.tue.nl/extra2/200612332.pdf)
[18] Hussain A K M F 1983 *Phys. Fluids* **26** 2816